# Propagation of geometric uncertainties in heat transfer problems solved by RBF-FD meshless method

Journal of Physics: Conference Series **1868** (2021) 012021 doi:10.1088/1742-6596/1868/1/012021

# Propagation of geometric uncertainties in heat transfer problems solved by RBF-FD meshless method

**R Zamolo, L Parussini and E Nobile**

Dipartimento di Ingegneria e Architettura, Università degli Studi di Trieste, via A. Valerio 10, 34127 Trieste, Italy

E-mail: rzamolo@units.it

**Abstract.** The design of engineering components must take into account the manufacturing tolerances of production processes since they lead to uncertainties in the behaviour of the products. It is therefore of valuable practical interest to quantify such uncertainties, with particular reference to problems involving geometrical uncertainties of the boundaries. This task is carried out in the present work by coupling the Non-Intrusive Polynomial Chaos (PC) method, employed for the quantification of uncertainties, with a Radial Basis Function Finite Differences (RBF-FD) meshless method, employed for the numerical simulations. The PC method with the Non-Intrusive formulation allows the use of existing deterministic solvers for the accurate prediction of the sought random response, i.e., the statistic moments of the involved variables. The RBF-FD method is therefore employed as a black box solver for the required set of problems defined over deterministic domains. The main advantage of the RBF-FD meshless method over traditional mesh-based methods is its capability of easily deal with practical problems defined over complex-shaped domains since no traditional mesh is required. The geometrical flexibility of the RBF-FD is even more advantageous in the context of geometric uncertainty quantification with the Non-Intrusive PC method since different solutions over different geometries are required. The applicability of the proposed approach to practical problems is then presented through the prediction of geometric uncertainty effects for a tube heat exchanger under natural convection where a 2D steady incompressible flow is considered.

## 1. Introduction

Tolerances and uncertainties in the manufacturing of generic products lead to an uncertain behaviour in their performances, which must be taken into account and accurately quantified when dealing with robust design. Therefore, it is of remarkable interest to develop efficient numerical approaches allowing the accurate quantification of such uncertainties in practical problems. In this work we deal with the propagation of geometric uncertainties on the boundaries in incompressible, laminar and steady-state fluid flows, focusing on the natural convection in a tube heat exchanger. The stochastic problem is solved by means of the Non-Intrusive Polynomial Chaos method [1-6]. The Non-Intrusive formulation [4,5] allows the use of existing solvers as black boxes without any modification since the calculation of the random response is based on a set of deterministic response evaluations. The use of the Polynomial Chaos formulation with particular orthogonal polynomials, e.g., Hermite polynomials,

allows the best representation of a given stochastic process, i.e., the number of required deterministic evaluations is minimum for any desired level of accuracy of the uncertainty [1,2]. The numerical solutions over the required deterministic geometries are obtained through a Radial Basis Function Finite Differences (RBF-FD) meshless method [6-12]. This choice is due to the geometric flexibility and the ability of RBF-FD meshless methods to easily deal with complex-shaped domains encountered in practical engineering problems: a traditional mesh/grid is no longer needed since a simple distribution of nodes over the domain is required. Futhermore, the employed Non-Intrusive formulation requires different numerical solutions over different geometries, which is a task that can be easily carried out by the RBF-FD method by means of a straightforward displacement of nodes [6]. The proposed approach is employed for the quantification of the statistical moments, i.e., expected value $\mu$ and variance $\sigma^2$, of some flow variables and related quantities, i.e., velocity, pressure, temperature, mass flow rate and local/mean Nusselt numbers over each tube, in the case of a 2D steady-state incompressible flow in a tube heat exchanger under natural convection with a Rayleigh number $Ra_D = 10^4$, based on the tubes diameter $D$. The horizontal (transverse) and vertical (longitudinal) tube pitches are described by two stochastic variables, while the validation of the deterministic RBF-FD solver is carried out on the same problem with $Ra_D = 2 \cdot 10^4$.

## 2. Nomenclature

The employed symbols are listed as follows:

| | | | |
|---|---|---|---|
| $a_j$ | RBF expansion coefficient | $T$ | temperature |
| $c_i$ | polynomial expansion coefficient | $\mathbf{u}$ | velocity vector |
| $D$ | tubes diameter | $\mathbf{u}^*$ | tentative velocity vector |
| $g_j$ | RBF polynomial basis | $u$ | horizontal velocity component |
| $Gr_D$ | Grashof number | $v$ | vertical velocity component |
| $h$ | reference size of node distribution | $W$ | tubes horizontal pitch |
| $H$ | tubes vertical pitch | $\mathbf{x}$ | position vector |
| $H_{in}$ | upstream domain extension | $\mathbf{x}_i$ | $i$-th node |
| $H_{out}$ | downstream domain extension | $\bar{\mathbf{x}}$ | mean position of supporting nodes |
| $m$ | dimension of RBF polynomial basis | $\Delta t$ | time step size |
| $\dot{m}$ | nondimensional mass flow rate | $\varepsilon$ | multiquadric RBF shape factor |
| $M$ | number of independent random variables | $\gamma_i$ | polynomial chaos basis functions |
| $n$ | number of RBF supporting nodes | $\mu$ | mean value |
| $N$ | total number of nodes | $\omega$ | multiquadric RBF |
| $\overline{Nu}_{D,i}$ | mean Nusselt number | $\Omega$ | physical domain |
| $p$ | pressure | $\varphi$ | random process |
| $P$ | polynomial basis degree | $\varphi_i$ | polynomial chaos expansion coefficients |
| $Pr$ | Prandtl number | $\Phi$ | projection auxiliary variable |
| $q$ | degree of Hermite polynomial | $\sigma$ | standard deviation |
| $Q$ | dimension of polynomial chaos basis | $\theta_i$ | random variables |
| $Ra_D$ | Rayleigh number | $\theta^{(i)}$ | zeros of Hermite polynomials |
| $s$ | spacing function | $\boldsymbol{\theta}$ | random vector |
| $t$ | time | $\vartheta$ | azimuthal angle |

## 3. Governing equations

Let us consider an incompressible fluid with density $\rho$, kinematic viscosity $\nu$, thermal diffusivity $\alpha$, thermal conductivity $k$ and volumetric temperature expansion coefficient $\beta$. The resulting conservation equations of mass, momentum and energy are

$$\nabla \cdot \boldsymbol{u} = 0 \tag{1}$$

$$\frac{\partial \boldsymbol{u}}{\partial t} + (\boldsymbol{u} \cdot \nabla)\boldsymbol{u} = -\nabla p + \frac{1}{\sqrt{Gr_D}}\nabla^2 \boldsymbol{u} + \boldsymbol{j}T \tag{2}$$

$$\frac{\partial T}{\partial t} + \boldsymbol{u} \cdot \nabla T = \frac{1}{Pr\sqrt{Gr_D}}\nabla^2 T \tag{3}$$

where $\boldsymbol{j}$ is the vertical unit vector. In the above equations, length, velocity $\mathbf{u} = (u, v)$, time $t$, pressure $p$ and temperature $T$ are made nondimensional by taking $D$, $U_0 = \sqrt{g\beta D\Delta T}$, $D/U_0$, $\rho U_0^2$ and $\Delta T$ as reference quantities, respectively, where $g$ is the gravitational acceleration. $Gr_D = g\beta D^3\Delta T/\nu^2$ is the Grashof number, $Pr = \nu/\alpha$ is the Prandtl number and $Ra_D = Gr_D \cdot Pr$ is the Rayleigh number.

## 4. Uncertainty quantification

### *4.1. Tensorial-expanded Polynomial Chaos*

Given a vector of $M$ independent random variables $\boldsymbol{\theta} = (\theta_1,\ldots,\theta_M)^T$, under certain conditions [2] a random process $\varphi(\mathbf{x},\boldsymbol{\theta})$ with finite second-order moments, which describes most physical processes, can be expanded as

$$\varphi(\mathbf{x},\boldsymbol{\theta}) = \sum_{i=0}^{\infty} \varphi_i(\mathbf{x})\gamma_i(\boldsymbol{\theta}) \tag{4}$$

where $\{\gamma_i\}$ is a suitable basis, $\varphi_i(\mathbf{x})$ are the corresponding expansion coefficients and $\mathbf{x}$ denotes the position. For each type of random variables distribution there exists the best representation, i.e., the best choice for the basis $\{\gamma_i\}$ in terms of convergence rate for the sought statistical moments of $\varphi$. In this work random variables with gaussian distribution $\theta_i \sim \mathcal{N}(0,1)$ will be considered only, therefore the corresponding best representation is given by Hermite polynomials (Hermite-Chaos) [1]. In fact, 1D Hermite polynomials are orthogonal with respect to the gaussian probability density function (PDF), therefore the $M$-dimensional tensorial-expanded Hermite polynomials are orthogonal with respect to the $M$-dimensional gaussian PDF $w(\boldsymbol{\theta})$ [1].

The expansion (4), expressed in the Hermite-Chaos form and truncated to a finite number $Q+1$ of terms, can be expressed as

$$\varphi(\mathbf{x},\boldsymbol{\theta}) = \sum_{i_1=0}^{q_1} \cdots \sum_{i_M=0}^{q_M} \varphi_{i_1\cdots i_M}(\mathbf{x}) H_{i_1}(\theta_1)\cdots H_{i_M}(\theta_M) \tag{5}$$

where $H_j(\theta)$ is the Hermite polynomial of degree $j$ (see [1] for further details).

The statistical moments of $\varphi$ can be computed from the approximation (5): the expected value $\mu(\varphi)$ and the variance $\sigma^2(\varphi)$ are

$$\mu(\varphi) = \int_{R^M} \varphi(\mathbf{x},\boldsymbol{\theta}) w(\boldsymbol{\theta}) d\boldsymbol{\theta} = \varphi_{0\cdots 0}(\mathbf{x}) \tag{6}$$

$$\sigma^2(\varphi) = \int_{R^M} [\varphi(\mathbf{x},\boldsymbol{\theta}) - \varphi_{0\cdots 0}(\mathbf{x})]^2 w(\boldsymbol{\theta}) d\boldsymbol{\theta} =$$
$$= -\varphi_{0\cdots 0}^2(\mathbf{x}) + \sum_{i_1=0}^{q_1} \cdots \sum_{i_M=0}^{q_M} \varphi_{i_1\cdots i_M}^2(\mathbf{x}) i_1! \cdots i_M! \tag{7}$$

### *4.2. Collocation*

In order to obtain the best approximation for $\mu(\varphi)$ and $\sigma^2(\varphi)$, we note that Eqs. (6)-(7) are weighted integrals with a gaussian weight function $w(\boldsymbol{\theta})$. Therefore, the best choice for the $Q+1 = (q_1+1)\cdots(q_M+1)$ sample points $\boldsymbol{\theta}^{(i)}$, i.e., the points where $\varphi(\mathbf{x},\boldsymbol{\theta})$ has to be evaluated, are the roots of the Hermite polynomial of degree $q_k+1$ along each of the $M$ dimensions, i.e., $H_{q_k+1}(\theta_k^{(i)}) = 0$ for $k = 1,\ldots,M$ and $i = 1,\ldots,q_k+1$. The Hermite-Chaos expansion (6) is therefore made valid at the previous $Q+1$ roots by using a collocation technique in order to obtain the $Q+1$ unknown coefficients $\varphi_{i_1\cdots i_M}(\mathbf{x})$. In other

words, the Hermite-Chaos expansion can be seen as an interpolant matching the random process $\varphi$ at the sample points $\boldsymbol{\theta}^{(i)}$.

## 5. RBF-FD meshless method

The evaluation of the random process $\varphi$ at the sample points $\boldsymbol{\theta}^{(i)}$ can be done with any suitable deterministic solver. Since the aim of this work is to analyze the effect of geometric uncertainties of the boundaries on the flow field, it is desirable to employ a solver which can easily and automatically address a specific fluid flow problem on different computational domains. In this perspective the RBF-FD meshless method is proposed.

### *5.1. RBF-FD discretization*

*5.1.1. 2D node distributions.* The 2D node distributions required by the RBF-FD meshless discretization have been obtained through the quadtree algorithm modified with a dithering correction, followed by repel refinement [13]. The resulting distribution is a set of $N$ nodes $\mathbf{x}_i$ which are isotropically displaced over the domain $\Omega$ and over its boundary $\Gamma = \partial\Omega$ according to a prescribed spacing function $s(\mathbf{x})$.

*5.1.2. RBF interpolation.* A generic field $\varphi$ is approximated near $\mathbf{x}$ by the following local RBF expansion

$$\varphi(\mathbf{x}) = \sum_{i=1}^{n} a_i \omega(||\mathbf{x} - \mathbf{x}_{i'}||) + \sum_{j=1}^{m} c_i g_j(\mathbf{x} - \bar{\mathbf{x}}) \tag{8}$$

where $i'$ are the indices of the $n$ supporting nodes $\mathbf{x}_{i'}$ closest to $\mathbf{x}$, $\bar{\mathbf{x}}$ is their mean position, $\omega(||\cdot||)$ are Radial Basis Functions (RBF) and $a_i$ are the corresponding coefficients. The functions $g_j$ form a complete 2D polynomial basis of degree $P$ with $m = \binom{P+2}{P}$ terms and $c_j$ are the corresponding coefficients. The chosen number of supporting nodes is $n=2m$ as suggested in [14-15]. The multiquadric RBF $\omega(r) = \sqrt{1 + (\varepsilon r)^2}$ has been chosen, where the shape factor is chosen to be $\varepsilon = 0.4/s(\bar{\mathbf{x}})$.

In order to express the coefficients $a_i$ and $c_j$ as functions of the nodal values of the unknown field $\varphi$, the expansion (8) is required to match φ at the supporting nodes which do not lie on the boundary, while boundary conditions are directly enforced at the supporting nodes lying on the boundary.

*5.1.3. RBF-FD collocation.* Given a linear partial differential equation $L(\varphi) = f$ in the unknown field $\varphi$, the RBF expansion (8) is made valid at each node $\boldsymbol{x}_k$ which does not lie on the boundary, obtaining a square and sparse linear system in the unknown nodal values $\varphi_k = \varphi(\mathbf{x}_k)$.

### *5.2. Solution procedure*

At each time step, the computation of velocity, pressure and temperature through Eqs. (1)-(3) is decoupled using a projection scheme with a three-level Gear scheme for the time discretization. A tentative velocity $\mathbf{u}^*$ is computed from the linearized momentum equation expansion

$$\frac{3\boldsymbol{u}^* - 4\boldsymbol{u}^l + \boldsymbol{u}^{l-1}}{\Delta t} + \boldsymbol{u}^l \cdot \nabla \boldsymbol{u}^* = -\nabla p^l + \frac{1}{\sqrt{Gr_D}} \nabla^2 \boldsymbol{u}^* + \boldsymbol{j} T^l \tag{9}$$

where $l$ is the time level and $\Delta t = 0.5$ is the chosen nondimensional time step size. $\mathbf{u}^*$ is then forced to satisfy the continuity equation (1) by means of an irrotational correction $\mathbf{u}^{l+1} = \mathbf{u}^* - \nabla\Phi$ , leading to the Poisson equation $\nabla^2\Phi = \nabla \cdot \mathbf{u}^*$ in the auxiliary variable $\Phi$.

The pressure is then updated as $p^{l+1} = p^l + \Phi / \Delta t$ and the temperature is computed from

$$\frac{3T^{l+1} - 4T^l + T^{l-1}}{\Delta t} + \boldsymbol{u}^{l+1} \cdot \nabla T^{l+1} = \frac{1}{Pr\sqrt{Gr_D}} \nabla^2 T^{l+1} \tag{10}$$

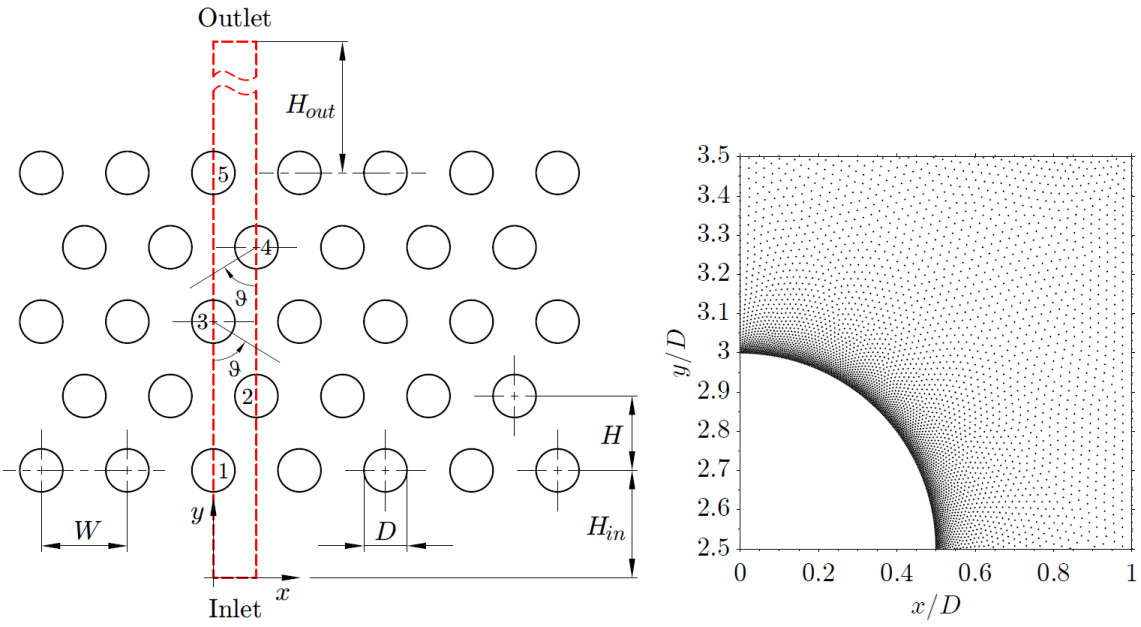


(a) (b)

**Figure 1.** Geometry of the problem (a), particular of a generated node distribution with $N$ = 84,167 nodes (b).

where $l$ is the time level and $\Delta t = 0.5$ is the chosen nondimensional time step size.
The previous equations are discretized with the same RBF-FD scheme presented in Section 4.1 employing a 6th order hyperviscosity stabilization [6]. A BiCGSTAB iterative solver [16], with an incomplete LU factorization as preconditioner [17], is employed for the solution of the transport Eqs. (9)-(10) using a relative tolerance $tol = 10^{-8}$, while the Poisson equation is solved through a LU decomposition which can be performed once at the beginning of the simulation. The steady-state convergence is declared when the normalized RMS time derivative of each flow variable, i.e., $u$, $v$, $p$ and $T$, is less than $10^{-5}$. The normalized RMS time derivative of a generic field φ is given by the RMS average of the numerical time derivative $(\varphi^{l+1} - \varphi^{l}) / \Delta t$, normalized by the amplitude A = max(φ) - min(φ).

## 6. Results

### *6.1. Problem definition*

The geometry of the problem is depicted in Figure 1, where the computational domain is indicated by the red hatched rectangle and extends $H_{in} = 2.5D$ below the lower tube (tube 1) and $H_{out} = 15D$ above the upper tube (tube 5). $W = 2D$ and $H = \sqrt{3}D$ are the horizontal and vertical tube pitches, respectively. Zero static pressure and zero normal derivatives for the velocities are imposed on both Inlet and Outlet, while symmetry conditions for both velocities and temperature are imposed at the vertical sides of the computational domain. $T = 0$ is imposed at the inlet and $T = 1$ is imposed at the tubes, while zero normal derivative for the temperature is imposed at the Outlet. A particular of a node distribution with $N$ = 84,167 nodes is also depicted in Figure (1): higher node density, i.e., number of nodes per unit area, is employed near the tube walls in order to accurately solve the wall gradients, especially for the temperature.

### *6.2. Validation of the RBF-FD method*

The implementation of the RBF-FD solver for this problem is validated for $Ra_D = 2 \cdot 10^4$. The convergence curves in terms of normalized RMS errors are depicted in Figure 2 for each of the flow

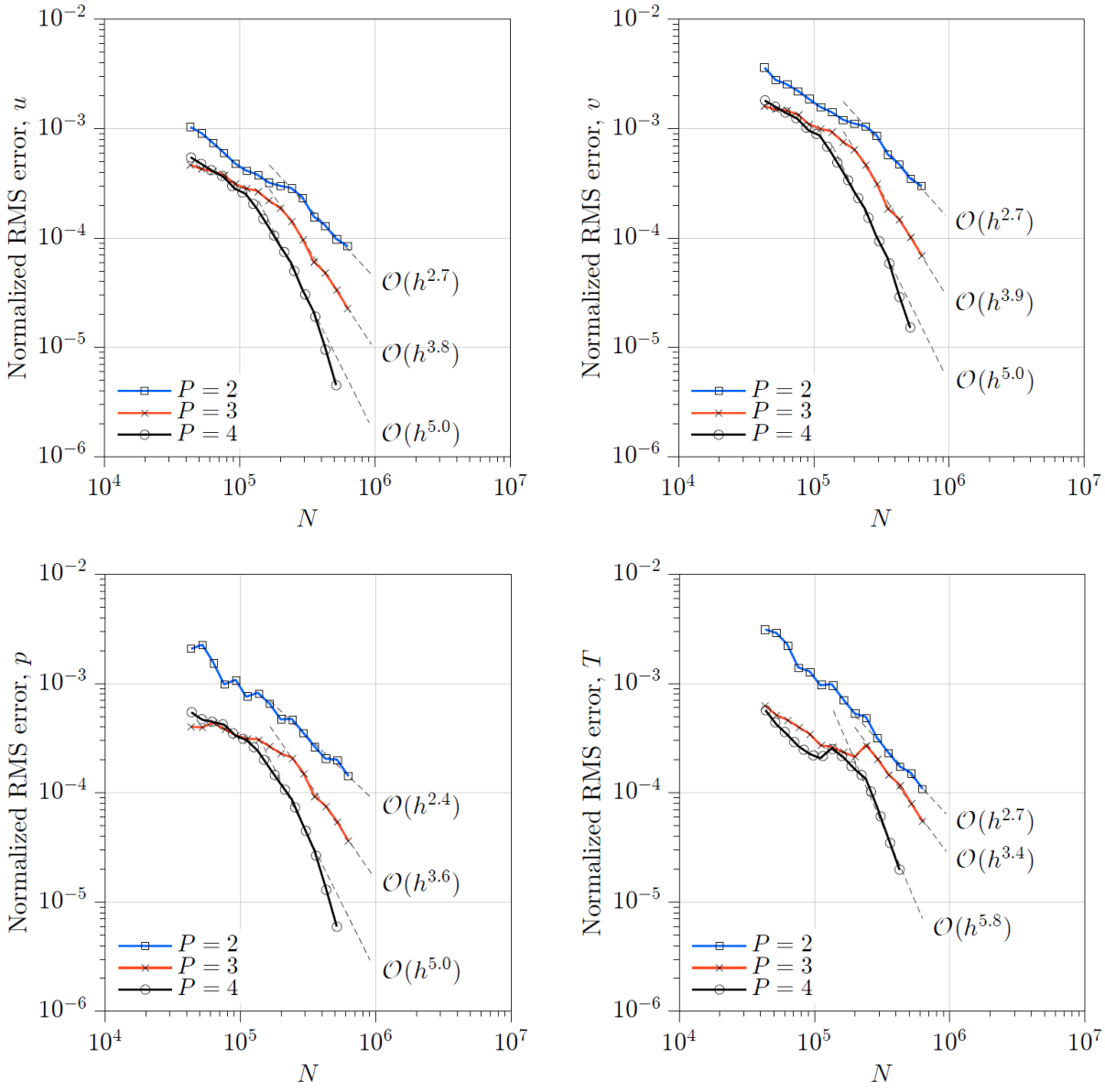


**Figure 2.** Convergence curves for the flow variables in the deterministic case at $Ra_D = 2 \cdot 10^4$.

variables and for three different polynomial degrees $P$ = 2, 3, 4 for the RBF expansion, where the numerical solution for $P$ = 4 and $N$ = 630,017 nodes is taken as reference. The resulting order of accuracy is approximately 2.5, 3.5 and 5.0 for $P$ = 2, 3, 4, respectively, which are obtained by taking the asymptotic linear regression curve using log-log scales. The last three simulations for $P$ = 4 are disregarded in the calculation of the linear regression curve since they would cause an overestimation of the order of accuracy. The convergence of the nondimensional mass flow rate $\dot{m}$ and mean Nusselt numbers $\overline{Nu}_{D,i}$ over each tube is reported in Table 1, where it can be appreciated the accuracy up to the third digit for almost each quantity.

**Table 1.** Convergence of some flow quantities in the deterministic case at $Ra_D = 2 \cdot 10^4$.

| | $N$ | $\dot{m}$ | $\overline{\mathrm{Nu}}_{D,1}$ | $\overline{\mathrm{Nu}}_{D,2}$ | $\overline{\mathrm{Nu}}_{D,3}$ | $\overline{\mathrm{Nu}}_{D,4}$ | $\overline{\mathrm{Nu}}_{D,5}$ |
|---|---|---|---|---|---|---|---|
| $P=2$ | 43,323 | 1.368 | 9.572 | 10.503 | 7.739 | 7.495 | 6.545 |
| | 92,049 | 1.370 | 9.579 | 10.525 | 7.721 | 7.475 | 6.504 |
| | 198,622 | 1.369 | 9.601 | 10.552 | 7.734 | 7.477 | 6.502 |
| | 425,457 | 1.369 | 9.621 | 10.556 | 7.732 | 7.477 | 6.499 |
| | 760,237 | 1.369 | 9.622 | 10.552 | 7.728 | 7.473 | 6.494 |
| $P=3$ | 43,374 | 1.371 | 9.589 | 10.550 | 7.711 | 7.458 | 6.477 |
| | 91,906 | 1.370 | 9.604 | 10.561 | 7.720 | 7.468 | 6.484 |
| | 198,851 | 1.369 | 9.615 | 10.559 | 7.725 | 7.472 | 6.490 |
| | 425,515 | 1.369 | 9.625 | 10.553 | 7.726 | 7.472 | 6.491 |
| | 760,201 | 1.369 | 9.626 | 10.551 | 7.726 | 7.472 | 6.491 |
| $P=4$ | 43,414 | 1.370 | 9.590 | 10.567 | 7.710 | 7.464 | 6.472 |
| | 92,083 | 1.369 | 9.607 | 10.560 | 7.722 | 7.469 | 6.486 |
| | 198,808 | 1.369 | 9.623 | 10.553 | 7.726 | 7.471 | 6.491 |
| | 425,365 | 1.369 | 9.626 | 10.549 | 7.726 | 7.471 | 6.491 |
| | 630,017 | 1.369 | 9.626 | 10.549 | 7.726 | 7.471 | 6.492 |

*6.3. Uncertainty quantification*

The uncertainty is introduced on the horizontal and vertical tube pitches. The horizontal pitch is chosen to be $W = 2D(1 + 0.05\theta_1)$ and the vertical pitch is chosen to be $H = \sqrt{3}D\ (1 + 0.05\theta_2)$, i.e., pitches with gaussian uncertainty characterized by 5% standard deviation. The uncertain space is therefore defined by $M = 2$ uncertain variables with normal distribution. Equal polynomial degrees $q_1 = q_2 = q$ are employed for the Hermite-Chaos expansion, requiring $Q+1 = (q_1 + 1)(q_2 + 1) = (q+1)^2$ deterministic RBF-FD solutions over the corresponding geometries. A lower Rayleigh number $Ra_D = 10^4$ is chosen in order to avoid flow instabilities originating from the recirculation zone above the upper tube for some of the required geometrical configurations. N ≈ 80,000 nodes are employed for the deterministic solutions over the required geometries.

The convergence of mean and standard deviation of the nondimensional mass flow rate $\dot{m}$ and mean Nusselt numbers $\overline{Nu}_{D,i}$ over each tube is reported in Table 3, where four different polynomial degrees $q = 1, 2, 3, 4$ for the Hermite-Chaos expansion are employed. A very fast convergence is achieved for the mean values and the standard deviation values are also apparently converging, although slightly more slowly. The zeros of the Hermite polynomials are listed in Table 2 for the employed values of $q$.

The normalized RMS errors for mean and standard deviation of the flow variables $u$, $v$, $p$ and $T$ are reported in Table 4, again for four different polynomial degrees $q = 1, 2, 3, 4$ for the Hermite-Chaos

**Table 2.** Zeros $\theta^{(i)}$ of the Hermite polynomial $H_{q+1}$ of degree $q+1$.

| $q$ | $\theta^{(i)}$ | | | | |
|---|---|---|---|---|---|
| 1 | | -1 | | 1 | |
| 2 | | -1.732 | 0 | 1.732 | |
| 3 | -2.334 | -0.742 | | 0.742 | 2.334 |
| 4 | -2.857 | -1.356 | 0 | 1.356 | 2.857 |

**Table 3.** Convergence of mean and standard deviation of some flow quantities in the stochastic case at $Ra_D = 10^4$.

| | $q$ | $\dot{m}$ | $\overline{\mathrm{Nu}}_{D,1}$ | $\overline{\mathrm{Nu}}_{D,2}$ | $\overline{\mathrm{Nu}}_{D,3}$ | $\overline{\mathrm{Nu}}_{D,4}$ | $\overline{\mathrm{Nu}}_{D,5}$ |
|---|---|---|---|---|---|---|---|
| Mean | 1 | 1.426 | 8.362 | 9.177 | 6.719 | 6.322 | 5.414 |
| | 2 | 1.426 | 8.362 | 9.176 | 6.718 | 6.321 | 5.413 |
| | 3 | 1.426 | 8.361 | 9.176 | 6.719 | 6.321 | 5.413 |
| | 4 | 1.426 | 8.362 | 9.176 | 6.718 | 6.321 | 5.413 |
| | | $[\times 10^{-2}]$ | $[\times 10^{-1}]$ | $[\times 10^{-1}]$ | $[\times 10^{-1}]$ | $[\times 10^{-1}]$ | $[\times 10^{-1}]$ |
| Std. Dev. | 1 | 4.011 | 0.764 | 0.635 | 0.997 | 0.624 | 0.949 |
| | 2 | 4.165 | 0.783 | 0.625 | 0.971 | 0.748 | 1.111 |
| | 3 | 4.163 | 0.772 | 0.613 | 0.964 | 0.769 | 1.129 |
| | 4 | 4.175 | 0.773 | 0.619 | 0.967 | 0.768 | 1.130 |

expansion. From this table it can be observed that the errors for the standard deviation values are strictly converging to the reference solution, which is obtained for $q = 4$, while the errors for the mean values are not strictly decreasing. In particular the errors of the mean values do not decrease when increasing the polynomial degree from $q = 2$ to $q = 3$. This is due to the fact that the reference solution for $q = 4$ is not the exact solution and the error due to the truncated Hermite-Chaos expansion is still present. Therefore, when the employed polynomial $q$ approaches the reference value $q = 4$, the relative difference is not fully reliable as an indicator of the real convergence. Nonetheless, from a practical point of view the absolute values of the normalized RMS errors for both mean and standard deviations are very small, confirming the high accuracy and efficiency of the Polynomial-Chaos collocation method.

The mean value and the standard deviation of the local Nusselt number over each tube are depicted in Figure 3, where it can be appreciated how the uncertainty on the pitches of the tubes has a stronger

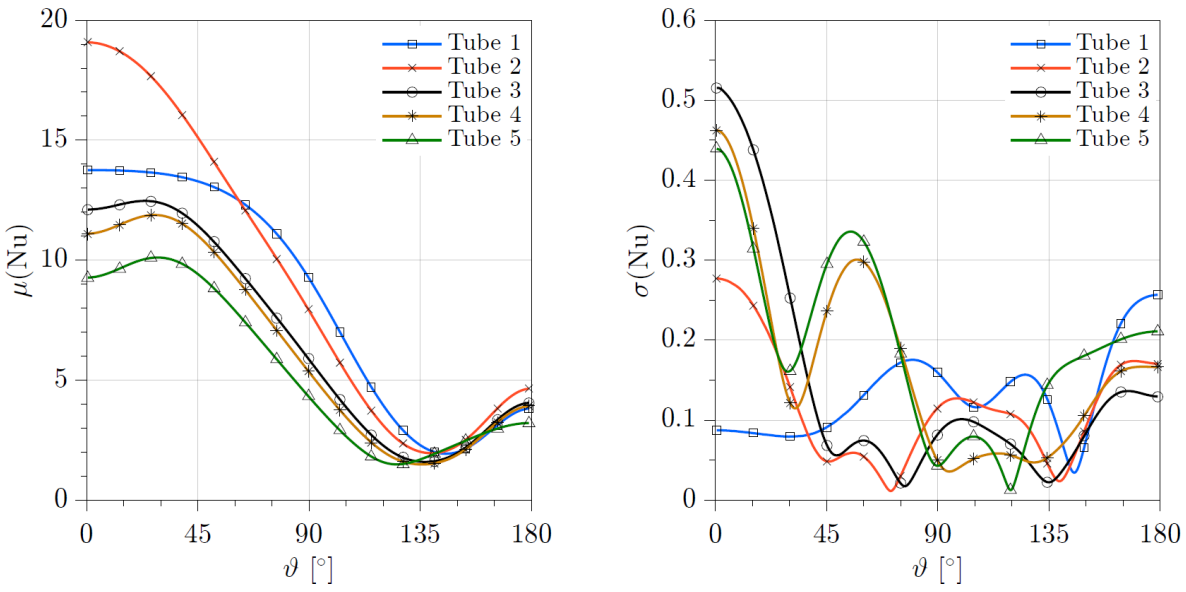


(a) (b)

**Figure 3.** Mean (a) and standard deviation (b) of the local Nusselt number for each tube at $Ra_D = 10^4$.

**Table 4.** Normalized RMS errors for mean and standard deviation of flow variables in the stochastic case at $Ra_D = 10^4$.

| $q$ | $\mu(u)$ $[\times 10^{-4}]$ | $\mu(v)$ $[\times 10^{-4}]$ | $\mu(p)$ $[\times 10^{-4}]$ | $\mu(T)$ $[\times 10^{-4}]$ | $\sigma(u)$ $[\times 10^{-2}]$ | $\sigma(v)$ $[\times 10^{-2}]$ | $\sigma(p)$ $[\times 10^{-2}]$ | $\sigma(T)$ $[\times 10^{-2}]$ |
|---|---|---|---|---|---|---|---|---|
| 1 | 0.361 | 1.047 | 0.444 | 0.831 | 0.623 | 1.310 | 0.642 | 1.167 |
| 2 | 0.043 | 0.129 | 0.169 | 0.087 | 0.056 | 0.140 | 0.053 | 0.096 |
| 3 | 0.225 | 0.923 | 0.281 | 0.354 | 0.021 | 0.052 | 0.030 | 0.017 |
| 4 | Ref. | Ref. | Ref. | Ref. | Ref. | Ref. | Ref. | Ref. |

influence on the local Nusselt number at low angles $\vartheta$ only for tubes 3, 4 and 5, while tubes 1 and 2 show a lower standard deviation at all angles, as confirmed by Table 3.

The mean value and the standard deviation of the flow variables are depicted in Figures 4 and 5 in the case $q$ = 4, where the streamlines are also shown. The streamlines reveal recirculation zones above each tube, where the standard deviation of the flow variables is low. As expected, zones with high standard deviation values for the velocities are encountered in between the tubes where the flow exhibits large gradients and large magnitudes in the velocities at the same time. The highest values of the standard deviation for the temperature is encountered in between tube 1 (lower tube) and tube 2, while zones with high standard deviation are also encountered in between the successive tubes, although with decreasing magnitude. On the contrary, the highest values for the pressure standard deviations are encountered along the vertical sides of the computational domain, halfway between the

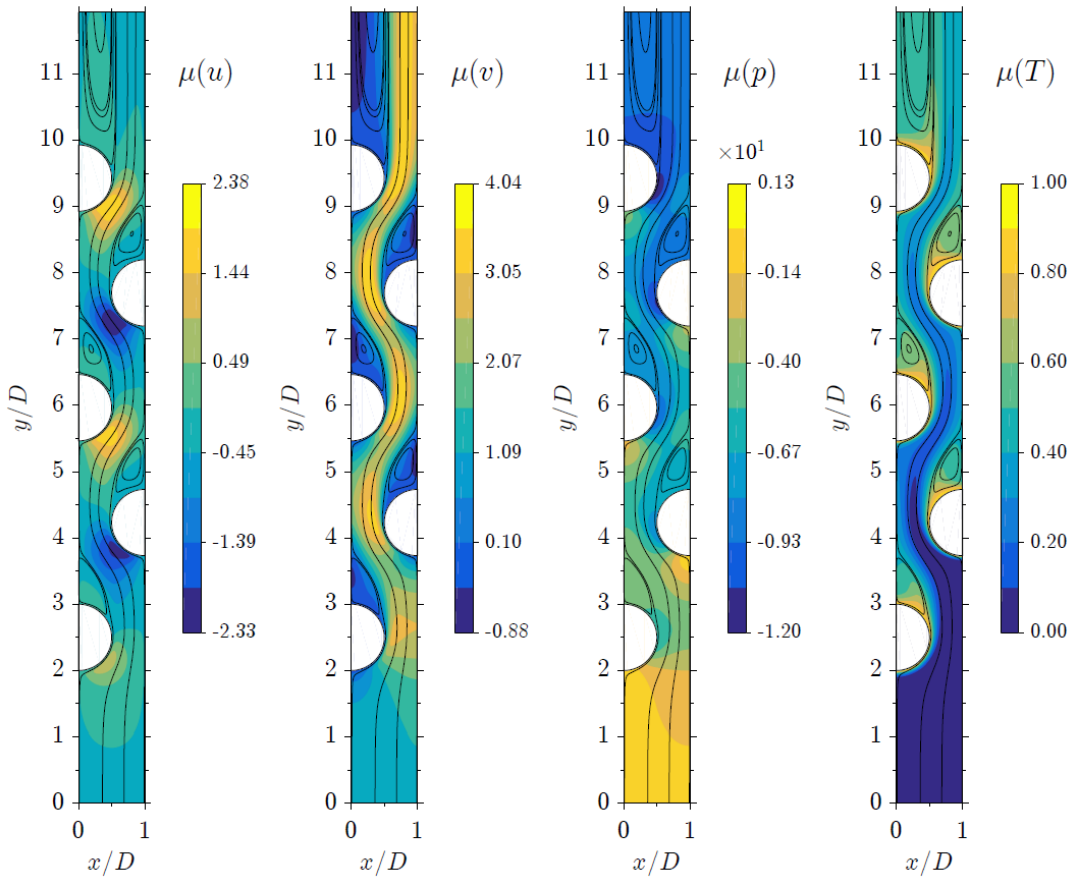


**Figure 4.** Mean value of the flow variables for $Ra_D = 10^4$ ($q$ = 4).

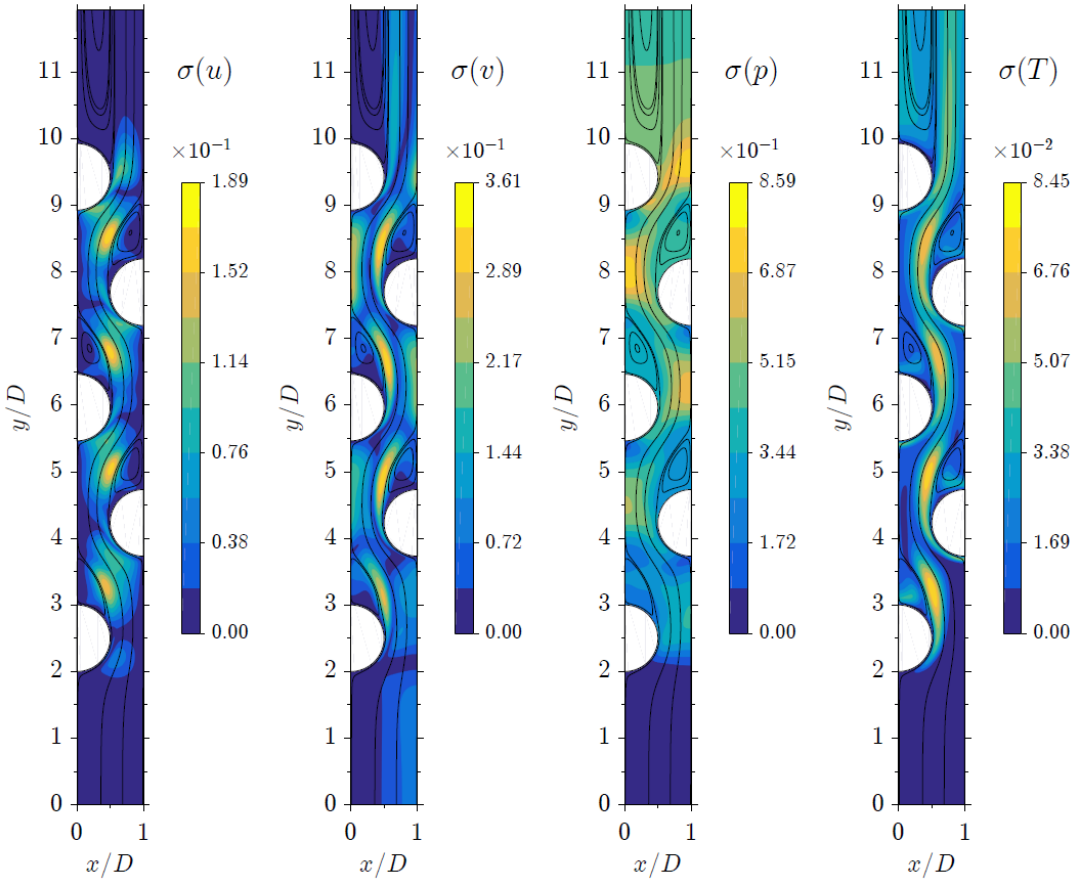


**Figure 5.** Standard deviation of the flow variables for $Ra_D = 10^4$ ($q = 4$).

tubes lying on the same side, which are the zones where the magnitude of the velocity is highest because of the reduced flow section.

## 7. Conclusions

In this work a Non-Intrusive Polynomial Chaos method is coupled to a RBF-FD meshless method for the accurate quantification of the uncertainties arising in laminar, incompressible and steady flows due to geometric uncertainties on the boundaries. The statistical moments of the sought flow quantities are evaluated with high accuracy by using the minimum number of deterministic fluid-flow solutions by means of the tensorial-expanded Polynomial-Chaos formulation in the case of a tube heat exchanger under natural convection. The main advantage of the presented meshless approach over standard mesh-based approaches is its capability to easily deal with complex geometries, which turns out to be an additional advantage when coupling the RBF-FD method to the employed Non-Intrusive Polynomial Chaos method since multiple deterministic solutions over different geometries are required. Furthermore, in addition to its geometrical flexibility, the RBF-FD method is a very promising choice since it is shown to be also very accurate and efficient, i.e., high orders of accuracy can be easily obtained.

Future work will deal with the extension of the presented methodologies to the deterministic and stochastic analysis of general heat transfer problems defined over 3D complex-shaped domains.

**References**

[1] Xiu D 2010 *Numerical Methods for Stochastic Computations* (Princeton University Press)
[2] Xiu D and Karniadakis G 2002 *SIAM J. Sci. Comput.* **24** 619-644
[3] Hosder S, Walters R and Perez R 2006 A Non-Intrusive Polynomial Chaos Method For Uncertainty Propagation in CFD Simulations *44th AIAA Aerospace Sciences Meeting and Exhibit, Reno, Nevada*
[4] Eldred M 2009 Recent Advances in Non-Intrusive Polynomial Chaos and Stochastic Collocation Methods for Uncertainty Analysis and Design *50th AIAA/ASME/ASCE/AHS/ASC Structures, Structural Dynamics, and Materials Conference, Palm Springs, California*
[5] Loeven G, Witteveen J and Bijl H 2007 Probabilistic Collocation: An Efficient Non-Intrusive Approach for Arbitrarily Distributed Parametric Uncertainties *45th AIAA Aerospace Sciences Meeting and Exhibit, American Institute of Aeronautics and Astronautics, Reston, Virigina, 2007*
[6] Zamolo R and Parussini L 2020 *J. Comput. Phys.* **421** 109730
[7] Li H and Mulay S 2013 *Meshless Methods and Their Numerical Properties* (CRC Press)
[8] Chinchapatnam P, Djidjeli K, Nair P and Tan M 2019 *Proceedings of the Institution of Mechanical Engineers, Part M: Journal of Engineering for the Maritime Environment* **223** 275-290
[9] Šarler B and Vertnik R 2006 *Comput. Math. Appl.* **51** 1269-1282
[10] Waters J and Pepper D 2015 *Numer. Heat Tr. B-Fund.* **68** 185-203
[11] Fornberg B and Flyer N 2015 *Acta Numer.* **24** 215-258
[12] Zamolo R and Nobile E 2019 *Numer. Heat Tr. B-Fund.* **75** 19-42
[13] Zamolo R and Nobile E 2018 *Comput. Math. Appl.* **75** 4305-4321
[14] Bayona V, Flyer N, Fornberg B and Barnett G 2017 *J. Comput. Phys.* **332** 257-273
[15] Bayona V, Flyer N and Fornberg B 2019 *J. Comput. Phys.* **380** 378-399
[16] van der Vorst H 1992 *SIAM J. Sci. Stat. Comp.* **13** 631-644
[17] Saad Y 2003 *Iterative Methods for Sparse Linear Systems* (SIAM, Philadelphia, Pennsylvania)